JOURNAL OF PROPULSION AND POWER
Vol. 26, No. 6, November–December 2010

# Experimental Study of Fluid Jet Mixing at Supercritical Conditions

Arnab Roy* and Corin Segal†
*University of Florida, Gainesville, Florida 32611*

DOI: 10.2514/1.48462

**Subcritical and supercritical fluids were injected in an inert gaseous atmosphere. Density distribution was measured and density-gradient profiles were inferred from the experimental data. A novel method was applied for the detection of detailed structures throughout the entire jet center plane. The core lengths were measured for each of the cases and correlated with previous visualization results. An eigenvalue approach was taken to determine the location of maximum gradients. The results show a significant influence of chamber-to-injectant density ratio on the core length in the supercritical domain, unlike the subcritical conditions.**

## Nomenclature

$D$ = injector diameter, 2 mm
$P$ = pressure, atm
$P_{cr}$ = critical pressure, atm
$P_r$ = reduced pressure
$T$ = temperature, K
$T_{cr}$ = critical temperature, K
$T_r$ = reduced temperature
$\rho$ = density, kg/m$^3$

## I. Introduction

THE problem of supercritical jet mixing is of significant importance since applications where high pressures and temperatures exist are extensive, including diesel and rocket engines where, often, the thermodynamic conditions exceed the fuel critical values. The inverse problem of a supercritical jet injected in subcritical conditions is also present, for example, in a supersonic combustion engine.

Liquid jet breakup in the subcritical regime has been extensively studied beginning with the pioneer theoretical works by Rayleigh [1], who suggested that a round liquid jet is not energetically stable and the instability onset leads, ultimately, to the jet disintegration. Rayleigh analyzed an inviscid, laminar, liquid jet and concluded that at the point of breakup, the characteristic drop diameter resulted as $d_d = 1.89d_l$, where $d_l$ is the jet diameter at the injector location. Further theoretical [2] and experimental studies [3] resulted in a number of semi-empirical expressions for the jet breakup length [4] and the resulting drop size distribution [5,6].

Incorporation of turbulence in the analytical investigation of the liquid round jet breakup has not been successful to date. The main reason is presumed to be the lack of detailed theory that could describe the turbulent shear layer with a sufficient degree of accuracy. The following should be noted:

1) If the jet is initially laminar, the breakup can be explained through the Kelvin–Helmholtz instability (KHI).

2) If the jet emerges turbulent from its injector, the KHI theory cannot explain the breakup and atomization [7].

The most significant feature of a supercritical fluid is the disappearance of surface tension; hence the term *liquid* is no longer applicable. The latent heat disappears and any fluid elements leaving the jet are governed by mass diffusion rather than evaporation.

Received 8 December 2009; revision received 1 July 2010; accepted for publication 3 July 2010. 

*Graduate Research Assistant. Student Member AIAA.
†Professor. Associate Fellow AIAA.

Experiments with fluid injected in a supercritical environment clearly illustrate the difference between subcritical and supercritical mixing, although the interpretation of the results may not be straightforward. Since following injection the fluid mixes with the surrounding gas the critical properties of the fluid cannot be considered as fixed values but dynamic parameters depending on the local conditions [8,9]. Experimental studies [9,10] suggested that, due to the disappearance of surface tension and vanishing of evaporation enthalpy, mixing between injected fluid and surrounding gas exhibits gas-gas mixing behavior once the critical values are reached. The absence of surface tension causes the diffusion process to dominate over the jet atomization.

Various computational studies [11–13] suggest that if the gas and jet densities are substantially different a supercritical jet behaves differently from its subcritical counterpart since the density difference causes turbulence damping. This causes it to have a longer unmixed core length compared with the turbulent subcritical gaseous jets [14].

To bridge the difference between numerical simulations and qualitative assumptions that can be derived from the available experimental results, Zong and Yang [15] pointed out that almost all of the available experimental information on supercritical jet mixing was obtained by using the shadowgraph technique, an experimental method that has several inherent restricting features. First, it is integrative: the light passes through the entire jet; therefore, the picture is an average throughout the jet. Second, the shadowgraph measures the density gradient, thus, the low density but highly turbulent regions can easily saturate the image. As a result, a relatively low density cloud of already mixed fluid which, indeed, exhibits gas-gas mixing features can hide the high density core.

In the current study planar laser-induced fluorescence was used to generate a section through the jet, thus accurately identifying both the boundary and the jet core structures. In the previous studies using the same facility [16,17] a jet at ambient temperature was injected into a chamber at supercritical conditions. Here, the jet was heated before injection into the chamber from subcritical to supercritical values. Three different regimes have been considered: 1) a subcritical jet into a subcritical environment, 2) a subcritical jet into a supercritical environment, and 3) a supercritical jet into a supercritical environment. The chamber-to-injectant density ratios ranged from 0.01 to 0.04. Further, the core lengths of the jet in all three regimes have been measured. In other studies, the core length has been defined as the length up to which an appropriate threshold intensity [18] exists, or measuring the location when the standard deviation of the pixel intensity of a row is zero. Since the definition of the core length is not unique among existing studies [19,20], an algorithm has been developed here to calculate the core lengths of the jet based on the change of density along the central portion of the jet. The core length data for all three regimes were plotted against chamber-to-injectant density ratio. The momentum ratio is often the selected parameter for comparing the core lengths for coaxial jets [19], but in the case of a

single jet, the density ratio becomes the relevant parameter. Analyses of core length data against the density ratio indicated differences between subcritical and supercritical conditions; these are explained below.

## II. Experimental Setup

The experimental setup is shown in Fig. 1. The schematic is shown in Fig. 1a and a picture of the setup is shown in Fig. 1b.

The details of the setup were given previously [21,22], hence only a brief description is included here. The high pressure chamber is built to withstand pressures up to 100 atm and temperatures up to 600 K. For optical access there are three windows with a field of view of 22 mm wide and 86 mm long. All experiments were done using a round liquid injector with a diameter of 2.0 mm. The flow is laminar before entering the injector and turbulence is not expected to develop while the fluid passes through the relatively short, 15.4 mm, injector tip. Nitrogen is used as the surrounding gas. Perfluoroketone, a 3M product, has been chosen as the injected fluid. The choice of this fluid was determined by its good spectroscopic properties and its low critical point: $P_{cr} = 18.4$ atm, $T_{cr} = 441$ K. Other material properties at standard temperature and pressure are as follows: density is 1608 kg/m$^3$, kinematic viscosity is 0.4178 cSt, surface tension is 0.01139 N/m. The third harmonic of Nd:Yag laser was used to excite the fluorescence. Earlier tests [17] have shown that emission spectrum of FK-5-1-12 within 400–500 nm does not reveal significant dependence on pressure and temperature within a range of interest. Based on emission spectra an optical filter with 420 nm centerline and 10 nm FWHM width was kept before the Princeton Instruments intensified charge-coupled device (ICCD) camera lens to eliminate any elastic scattering. The ICCD camera has a resolution of 512 × 512 pixels; it was cropped to 311 × 512 pixels to increase the acquisition rate to 10 Hz and to synchronize it with the laser. The gate width was kept to 150 ns to capture the entire duration of fluorescence while reducing the background light significantly.

A thin laser sheet of 0.1 mm thickness and 25 mm length was focused on the jet centerline. The intensity of the emitted fluorescence was directly proportional to the local density of the jet. The images of the jet were scaled and analyzed to determine the core lengths.

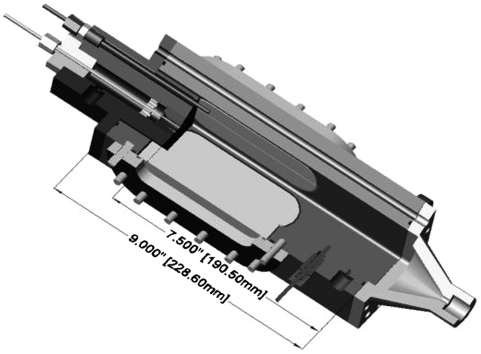


a)

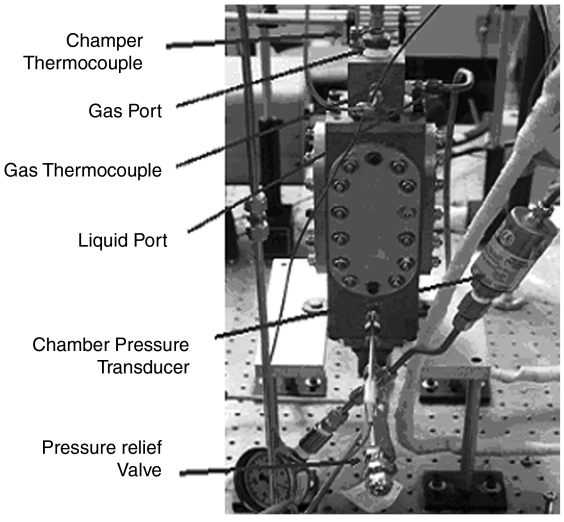


b)

**Fig. 1 Test chamber a) schematic and b) overall view. The figure shows the position of the thermocouples and the pressure transducer connected to the chamber. The liquid and gas injection ports are also indicated. The 25 mm square chamber with 228 mm length can be heated and pressurized to 600 K and 100 atm respectively. It features a single 2 mm diameter injector at the top end.**

## III. Results and Discussion

### A. Experimental Conditions

The experimental conditions are shown in Fig. 2 on a reduced pressure ($P_r$) and reduced temperature ($T_r$) diagram. The goal was to span a range of pressures at constant temperature, with particular focus in the supercritical zone. Thus, a very wide range of temperatures and pressures have been covered. Previous studies [23] have shown that supercritical behavior may be encountered even when only one of the parameters, $P_r$ or $T_r$, is critical. Therefore, a sweep of pressures for given temperatures were selected along with conditions that kept the pressure essentially constant and increased the temperature. Both the chamber and the injectant conditions are shown on the diagram separately.

The experiments have been categorized under three subgroups: 1) a subcritical jet being injected into a subcritical environment, 2) a subcritical jet into a supercritical environment, and 3) a supercritical jet into a supercritical environment. The images obtained in each category have been analyzed and density profiles have been obtained to identify the differences of the three breakup and mixing regimes. Moreover, the core lengths of the jet in each of these cases have been compared with evaluate the effects of pressure and temperature on the breakup of the jet.

In the following sections the measurement of the core length shall be explained followed by the discussion and comparison of the core lengths for each of the three cases of injection.

### B. Core Length Measurement Algorithm

The term *core length* usually refers to the intact section of the jet which is higher in density than the remaining areas. The core length does not have any unique definition among researchers. Various terms such as the intact length, potential core, and breakup length have been used along with various measurement techniques to determine the same, as mentioned in previous studies [18,19]. The core length is defined here as the intact section of the jet, measured

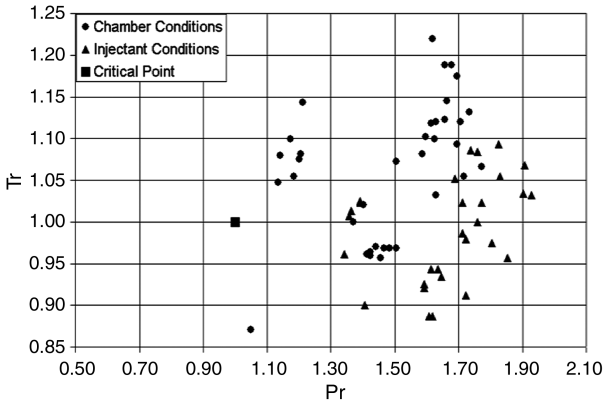


**Fig. 2 Selection of the experimental conditions. Reduced temperatures and pressures have been selected to cover the subcritical to supercritical regime. The plot refers to both the chamber and the injectant conditions independently. The selected combinations will be emphasized in the following sections discussing the results.**

along its axial length, beyond which a considerable change of density occurs. The core lengths were calculated for the chamber-to-injectant density ratios from 0.01 to 0.04.

The algorithm developed here to calculate the core length starts with a single jet image. The image is scaled using the pixel intensities as shown in Fig. 3. Each shade in the scaled image corresponds to a local density range. Thus the brightest pixel corresponds to the highest density. The analyzed images are stored as a matrix of local density values which is then used for determining the core length.

The first row of the density matrix is scanned to find the width of the jet at the injector. This width is used to create individual square density matrices or blocks along the entire length of the jet, where each block starts one row after the previous block as shown in Fig. 3a. The average and the eigenvalues of each of these matrices are then computed. The determinants of the eigenvalue matrices are plotted in Fig. 3b. A polynomial is fitted to this plot and its points of inflexion correspond to a significant change in density across the axial length of the jet. At each point of inflexion the average density matrix is compared with its neighboring ones. The point that corresponds to the maximum density change with respect to its immediate neighbors is taken to be the core length. As can be seen from Fig. 3b, the point of inflexion between pixel number 300 and 400 is found to be the core length, and it is shown in Fig. 3c.

For each experiment, the core lengths were calculated for all images, then an average of this value was taken. It should also be noted that this method of calculating the core length is sensitive to core separation; hence the length before separation is taken to be the core. In some cases, the method overpredicts the core length due to the approximation involved in fitting the polynomial and calculating the points of inflexion, and hence these cases have been discarded.

Since the core length does not have a unique definition among researchers [24], different measuring techniques [25,26] can change its absolute magnitude. Thus, more emphasis should be made on the trends that they have with different operating conditions. In the sections that follow, core length has been plotted as a function of the chamber-to-injectant density ratio, ranging from 0.01 to 0.04. Trend lines have been fitted to two of cases, and it can be seen that the core length for the supercritical injections change more rapidly than the subcritical injection, indicating that the supercritical cases have a stronger dependence on density ratio than the subcritical cases. This observation is similar to that of coaxially injected jets [18,19], where the core lengths have been plotted as a function of momentum flux ratio and a trend for the core lengths has been observed.

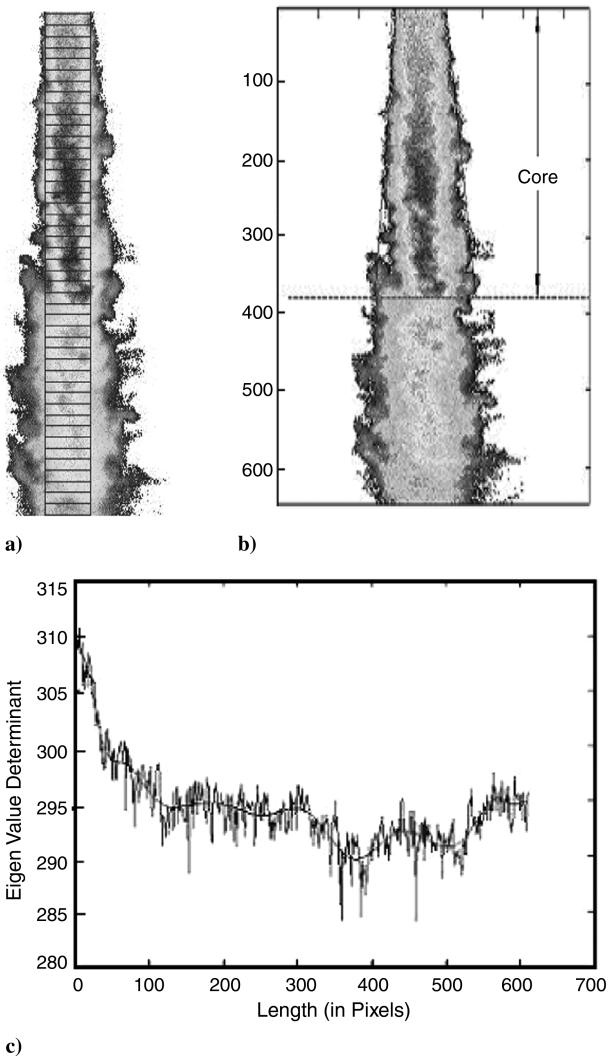


**Fig. 3 Basis for core length determination: a) portion of the jet where individual density matrices or blocks are chosen, depicted by shaded area, b) calculated core length, and c) determinants of the eigenvalue matrices plotted against pixel length.**

### C. Subcritical Fluid into a Subcritical Atmosphere

The experiments done under these conditions involve relatively lower temperatures for the injectant and the chamber. The temperatures for the injected fluid ranged from 343 to 423 K, while the temperature of the surrounding atmosphere ranged from 383 to 428 K. This represents $T_r$ values ranging from 0.78 to 0.96 for the injected fluid, and 0.87 to 0.97 for the chamber, both subcritical with respect to the critical temperature of 441 K for the injectant. The pressures were kept higher than the critical pressure of 18.4 atm and were in the range of 20 to 30 atm for both the injectant and surroundings representing $P_r$ ranging from 1.09 to 1.63. Hence, the injected fluid was always injected into the chamber as a compressed liquid instead of a superheated vapor. At lower pressures the injectant could become superheated vapor, undergo a constant pressure cooling process on the windows, and cause a condensation of the vapor on the windows resulting in subsequent absorption of the laser sheet and a reduction of fluorescence. To avoid these problems the pressures for all experiments were kept higher than the critical pressure. The injection velocity ranged from 5.9 to 8.4 m/s. for this case.

The processed images of the fluid at subcritical conditions injected into a subcritical atmosphere are shown in Fig. 4. The images are taken for 10 jet diameters from the injector. It can be observed that surface tension and inertia forces dominate under these conditions with droplet formation observed once the fluid detaches from the jet. Since the observation was conducted for first 10 jet diameters from the injector and the jet was initially laminar droplet formation was

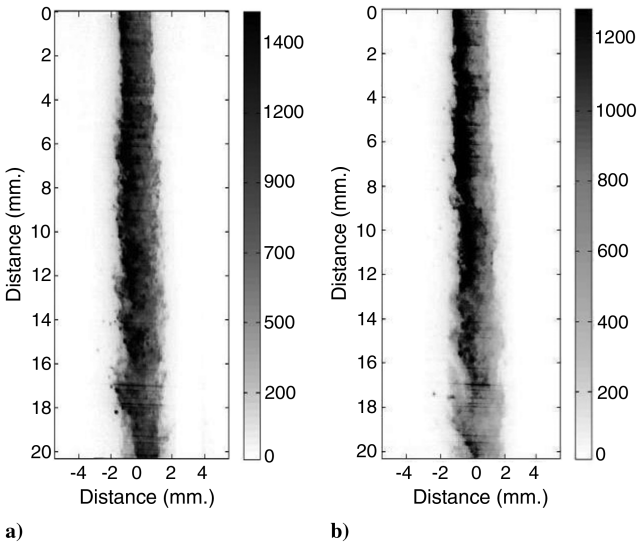


**Fig. 4 Scaled images of a subcritical jet injected at subcritical chamber conditions: a) jet initially at $Tr = 0.79$, $Pr = 1.57$ injected into the chamber at $Tr = 0.96$, $Pr = 1.41$ at a velocity of 5.9 m/s and b) jet initially at $Tr = 0.89$, $Pr = 1.61$ injected into the chamber at $Tr = 0.97$, $Pr = 1.47$ at a velocity of 5.9 m/s.**

rarely observed within the portion shown in the figures. However, the occasionally observed droplets had an ellipsoid or round shape, i.e., the surface tension forces were relatively strong. Pronounced ligament formation is observed under these conditions. As used here, a ligament is a distinct protrusion from the surface of the liquid jet caused by the interface shear. They appear with certain periodicity and correspond to the surface waviness caused by instabilities. In the figure shown below, droplet formation can be seen towards the lower portion of the jet when injected at lower injectant temperatures.

The experimental conditions for this case have been plotted in Fig. 5 on a reduced temperature and reduced pressure diagram. The chamber and injectant conditions have been shown separately and have been numbered in pairs to evidence that the chamber conditions have been kept relatively close to each other, while the injectant conditions vary in temperature and pressure, so a range of chamber-to-injectant density ratios could be covered.

The injection velocity for these cases ranges from 5.9 to 8.4 m/s. Hence, the density ratio has been chosen as the most significant parameter to compare the core lengths. Figure 6 shows how the core length varies with the density ratio. The numbers shown in the plot correspond to the experimental conditions shown in Fig. 5. It can be concluded from the plots that for a wide range of density ratios, the core length remains unchanged and seems to be independent of the density ratio as long as the velocities are kept similar for all cases.

There can be changes in the core length due to injection velocity variations. In this study, the injection velocity of the jet was kept essentially the same for all cases to isolate the effect of the density ratio on the variation of the core length.

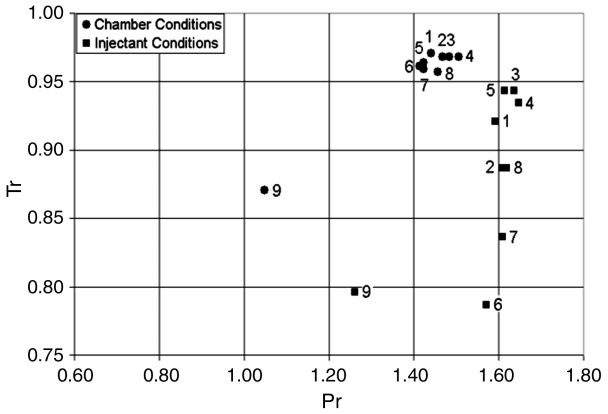


**Fig. 5 Selection of experimental conditions. Chamber and injectant conditions have been shown separately and have been numbered in. The chamber conditions have been kept relatively close to each other, while the injectant conditions vary in temperature and pressure. Hence, a wide range of chamber-to-injectant density ratios could be covered.**

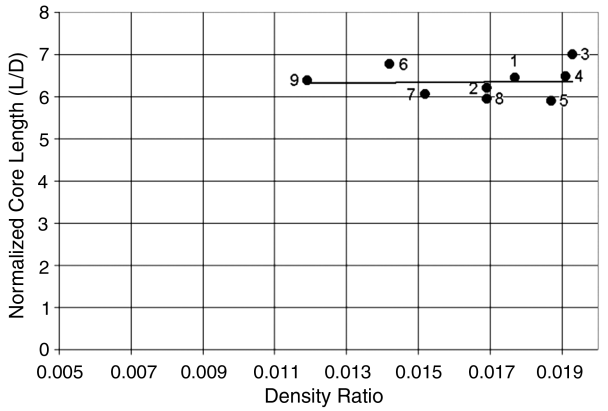


**Fig. 6 Plot of the core length versus the chamber-to-injectant density ratio. The numbers correspond to those of the previous plot. The figure indicates for this case, the core length values are quite independent of density ratio for little or no variations of injection velocities.**

### D. Subcritical Fluid into a Supercritical Atmosphere

Here, the temperature for the injected fluid ranged from 291 to 435 K while the temperature of the surrounding atmosphere ranged from 441 to 538 K. This represents $T_r$ values ranging from 0.66 to 0.99 for the injected fluid and 1 to 1.22 for the chamber. The pressures were again kept higher than the critical pressure of 18.4 atm and were in the range of 20 to 35 atm for both the injectant and surroundings, which represent $P_r$ values ranging from 1.09 to 1.90. The injection velocity ranged from 5.3 to 10.2 m/s.

The images of the jet injected at subcritical conditions into a supercritical atmosphere can be seen in Fig. 7. The characteristic feature of this region is the apparent decreased importance of surface tension that manifests through the smoothening of the liquid-gas interface. Ligament formation tends to significantly decrease. Because of the decreased surface tension forces, the ligaments have a cluster or fingerlike appearance from which parcels of liquid detach, the shape of which is similar to the previous studies [27]. At lower injectant temperatures, the surface of the jet corrugated and wavy, and some of the clusters get detached from the main body of the jet and form drops. At higher injectant temperatures, the surface becomes smoother and drops are no longer observed.

The experimental conditions have been plotted for this case on a reduced temperature and reduced pressure diagram, as shown in Fig. 8. Certain test conditions have been circled because they correspond to specific conditions that allow the analysis of the results as shown below.

As can be seen from Fig. 8, the chamber conditions and injectant temperature are quite similar for cases 11 and 12. The only parameter that is different is the injectant pressure, which is higher in 11 than in 12. Figure 9 shows that this causes the core length to be shorter in case 12 than in 11 indicating that a rise in injectant pressure causes a lengthening of the core caused, mostly, by increased jet density.

Further, Fig. 8 shows that the injectant conditions and chamber pressure are similar for cases 4 and 9, whereas, the chamber temperature is quite different: case 4 has a higher chamber temperature than case 9. Figure 9 shows that the core length for case 4 is much higher than in case 9, which indicates that a decrease in chamber temperature causes a shortening of the core length. A similar argument can be made for cases 7 and 10 where the injectant conditions are almost the same while the chamber conditions are different. The chamber pressure is lower in case 10, which causes it to have a higher core

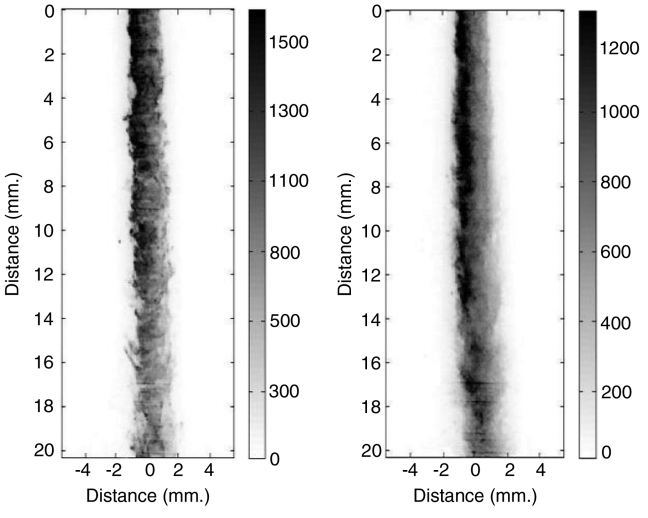


a) b)

**Fig. 7 Scaled images of a subcritical jet injected at supercritical chamber conditions: a) jet initially at $Tr = 0.66$, $Pr = 1.85$ injected into the chamber at $Tr = 1.19$, $Pr = 1.68$ at a velocity of 5.3 m/s and b) jet initially at $Tr = 0.91$, $Pr = 1.72$ injected into the chamber at $Tr = 1.02$, $Pr = 1.40$ at a velocity of 10.1 m/s.**

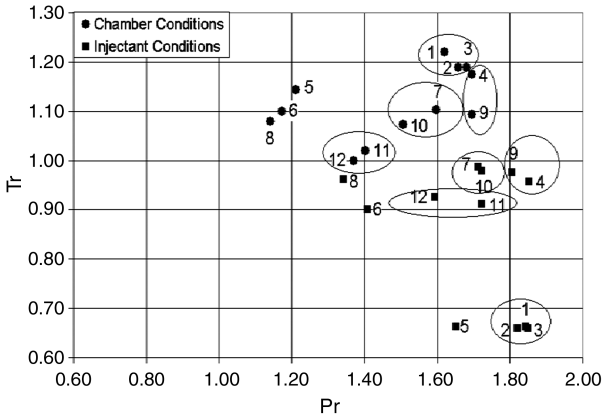


**Fig. 8 Plot showing the range of experimental conditions. Chamber and injectant conditions have been shown separately. Certain test conditions have been circled to analyze how the core lengths change with temperature and pressure when one is kept fixed and the other is varied.**

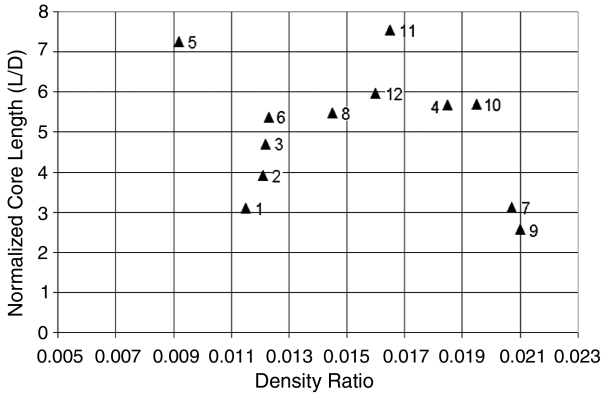


**Fig. 9 Plot showing the core lengths against the chamber-to-injectant density ratio. The numbers correspond to those of the previous plot.**

length than case 7. Thus, the chamber pressure rise causes a shortening of the core length.

Finally, cases 1, 2 and 3 are considered. Figure 8 shows that they have almost identical test conditions, though the core length values do not seem similar. This discrepancy can be attributed to the injection velocity differences, which ranged between 5.3 to 6.6 m/s. Case 1 has the highest injection velocity, which causes greater shear at the jet edges and causes it to have the lowest value for the core length, while lower injection velocities for cases 2 and 3 induce lower core length values.

### E. Supercritical Fluid into Supercritical Atmosphere

The chamber temperatures ranged in these cases from 455 to 505 K, while the injectant temperatures ranged from 441 to 482 K. This represents $T_r$ values ranging from 1 to 1.09 for the injected fluid and 1.03 to 1.15 for the chamber. The pressures for both the chamber and the injectant ranged from 22 to 36 atm, which represent $P_r$ values ranging from 1.20 to 1.96 that are well beyond the critical temperature of 18.4 atm for the injectant.

In the supercritical zone, as shown in Fig. 10, the jet behavior changes considerably. Shear forces now exceed the capillary forces and they dominate. The density-gradient magnitudes continue to decrease. Ligaments are considerably reduced and appear as thin material threads emanating from the jet that later dislocate in irregular shapes. Because of interactions at the surface, instabilities lead to disturbances that manifest as surface waves. In the regime when the surface tension is significant, hydrodynamic instability leads to the spatial development of these waves and the eventual jet breakup. Characteristic disturbance waves correspond to the

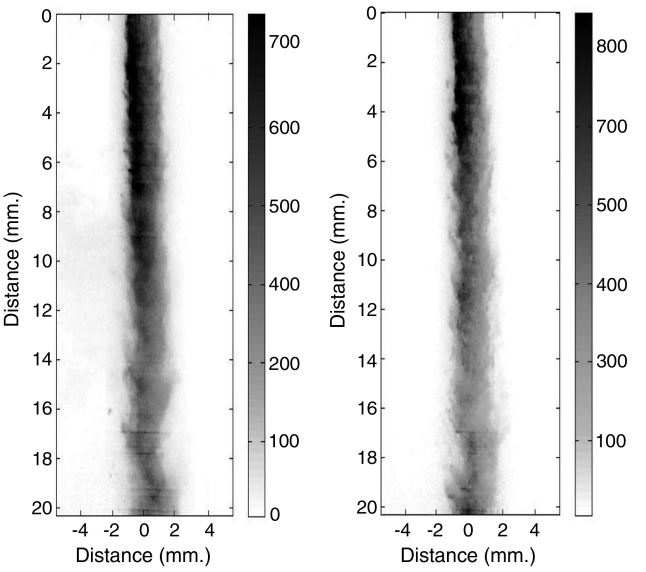


a) b)

**Fig. 10 Scaled images of a supercritical jet injected at supercritical chamber conditions: a) jet initially at $Tr = 1.01$, $Pr = 1.36$ injected into the chamber at $Tr = 1.07$, $Pr = 1.20$ at a velocity of 10.7 m/s and b) jet initially at $Tr = 1.02$, $Pr = 1.71$ injected into the chamber at $Tr = 1.10$, $Pr = 1.63$ at a velocity of 6.5 m/s.**

resonant frequencies of the system consisting of liquid and gas inertia and surface tension forces. Once the surface tension is reduced, as the critical conditions are reached and exceeded, these mechanisms yield to other forms of energy exchange between the jet and the gaseous surroundings; among the possible destabilizing mechanisms at these conditions, the KHI is expected to dominate. The jet mixing would eventually approach a liquid/liquid or a gas/gas like mixing at very high temperatures and pressures. In certain cases, it is seen that the core length decreases significantly than the previous two injection cases.

The experimental conditions are shown in Fig. 11 on a reduced temperature and reduced pressure diagram. The chamber and injectant conditions have been shown separately and numbered as for the previous cases. Experiments with similar test conditions for both the chamber and the injectant have been circled for easy identification. The analysis that follows is based on the effect of the test conditions on the core length.

Cases 9 and 10 in Fig. 11 have similar injectant and chamber conditions, and thus their chamber-to-injectant density ratios are close. Figure 12 shows the core lengths in cases 9 and 10 indicating that these are quite similar. Moreover, other similar cases like 11 and

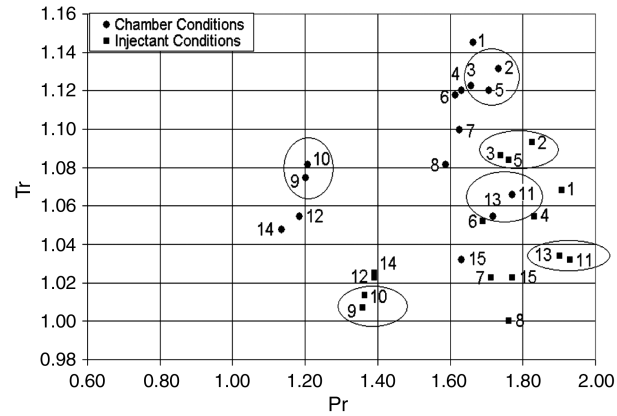


**Fig. 11 Selection of experimental conditions. Both the injectant and the chamber conditions have been shown on a reduced temperature and reduced pressure diagram. Similar experimental conditions have been circled for easy identification.**

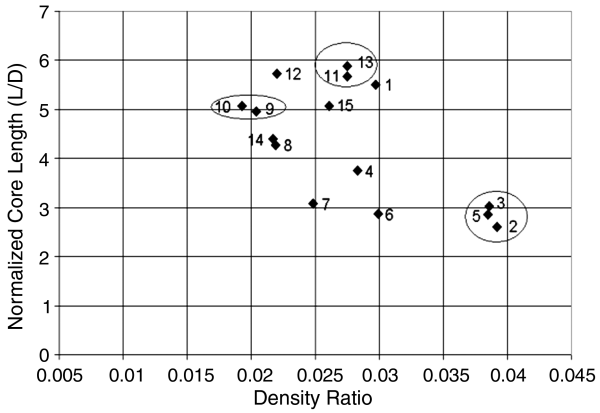


**Fig. 12 Plot showing the core lengths against the chamber-to-injectant density ratio. The numbers correspond to those of the previous plot. Similar experimental conditions have been circled and can be seen to have similar core lengths.**

13 also show that the core lengths are quite close. In case 11, however, the chamber temperature and pressure was slightly higher than case 13 causing the core length to be slightly shorter than case 13.

Cases 3 and 5 have very similar test conditions, which also causes them to have very similar core lengths, as can be seen from Fig. 12. Case 2, on the other hand, has higher temperatures and pressures for both the chamber and the injectant than cases 3 or 5. The chamber-to-injectant density ratio is also slightly higher in case 2 and this causes the core length to be shorter than the other two cases. The cases stated above also verify the accuracy of the tests, since the tests repeated with similar conditions produce similar core lengths.

To find out the effects of the chamber or injectant conditions on the core length, cases 7 and 15 are chosen. The injectant conditions for these are nearly the same. The chamber pressures are also quite similar, but the chamber temperatures are significantly different. This results in different core lengths, as can be seen from Fig. 12. Thus, it can be inferred that at similar injectant conditions and chamber pressures, the core length increases with decreasing chamber temperature. This effect is exactly opposite to what was observed for a subcritical jet injected into a supercritical atmosphere. Cases 4 and 6 indicate that the chamber conditions and injectant temperature for these cases are nearly the same but the injectant pressure is higher in case 4. This causes a higher density ratio and, hence, a higher core length for case 4 than case 6. Thus, it can again be concluded, that at similar chamber conditions and injectant temperatures, the core length increases with increasing injectant temperature.

From this analysis, it is concluded that the most significant parameter that affects the core length is the chamber-to-injectant density ratio. It should also be noted that the velocity can also be a significant parameter in determining the core length. The velocity ranges that were dealt with in these experiments were quite narrow to affect the core length in a significant way.

## IV. Conclusions

1) A study of a heated jet injected into a gaseous environment was undertaken at three separate conditions: a subcritical jet into a subcritical atmosphere, a subcritical jet into a supercritical atmosphere, and a supercritical jet into a supercritical atmosphere.

2) The images obtained using planar laser-induced fluorescence through the jet core. This method of image acquisition has significant advantages over shadowgraph techniques, which is integrative since it passes through the entire jet.

3) The images indicate the characteristics of subcritical and supercritical mixing as mentioned in the theories. In the case of a subcritical jet injected into a subcritical environment, surface tension and inertia forces dominated the jet breakup process, and droplet formation was observed when the portions of the jet broke off.

4) In the case of subcritical jet injected into a supercritical environment, the surface of the jet became smoother than in the previous case, and both droplet formation and irregularly shaped material were observed when a portion of the jet broke off.

5) In the case of a supercritical jet injected into a supercritical environment, the jet surface changed completely. Surface tension disappeared, and the surface became smooth with minimal irregularities. With increased temperature and pressure, the density-gradient values decrease.

6) The core lengths have been calculated for various conditions of the chamber and injectant. The method developed for calculating the core lengths is an eigenvalue approach as described above to identify the points of maximum density gradient. The method gives good results and also helps to identify the point of core separation, though it tends to overpredict the core length in certain cases.

7) The core lengths were plotted as a function of the density ratio for all cases, since in the absence of any momentum ratio, the density ratio is the most important parameter for comparison if the velocities do not significantly change between experiments.

8) In the subcritical-into-subcritical case, it was observed that the core length remains essentially unaffected by the density ratio for density ratios ranging from 0.01 to 0.02.

9) In the subcritical-into-supercritical case, the core length changes quite strongly with density ratio, but no definite pattern could be observed. The range of density ratios covered for this case was from 0.009 to 0.021.

10) In the supercritical-into-supercritical case, the core length again shows a strong dependence on the density ratio. The core length tends to decrease with an increase in density ratio. All the tests were done for density ratios varying from 0.019 to 0.04.

11) These results are similar to the other experiments involving observations for coaxial jets, where the core length has been plotted against momentum ratio. It has been found there that the core length has a stronger dependence on momentum ratio in the supercritical-into-supercritical cases than in the subcritical-into-supercritical or subcritical-into-subcritical cases.

## References

[1] Rayleigh, L., "On the Instability of Jets," *Proceedings of the London Mathematical Society*, Vol. s1-10, No. 1, 1878, pp. 4–13. doi:10.1112/plms/s1-10.1.4

[2] Weber, C., "Disintegration of Liquid Jets," *Journal of Applied Mathematics and Mechanics*, Vol. 11, No. 2, 1931, pp. 136–159.

[3] Haenlein, A., "Disintegration of a Liquid Jet," NACA TN 659, 1932.

[4] Grant, R. P., and Middleman, S., "Newtonian Jet Stability," *AIChE Journal*, Vol. 12, No. 4, 1966, pp. 669–678. doi:10.1002/aic.690120411

[5] Sterling, A. M., and Sleicher, C. A., "The Instability of Capillary Jets," *Journal of Fluid Mechanics*, Vol. 68, No. 3, 1975, pp. 477–495. doi:10.1017/S0022112075001772

[6] Dan, T., Yamamoto, T., Senda, J., and Fujimoto, H., "Effect of Nozzle Configuration for Characteristics of Non-Reacting Diesel Fuel Sprays", Society of Automotive Engineers Paper 970355, 1997.

[7] Lin, S. P., *Breakup of Liquid Sheets and Jets*, Cambridge Univ. Press, Cambridge, England, U.K., 2003.

[8] Chehroudi, B., and Talley, D. G., "The Fractal Geometry of Round Turbulent Cryogenic Nitrogen Jets at Subcritical and Supercritical Pressures," *Atomization and Sprays*, Vol. 14, No. 1, 2004, pp. 50–60.

[9] Oschwald, M., Smith, J. J., Braman, R., Hussong, J., Schik, A., Chehroudi, B., and Talley, D. G., "Injection of Fluids into Supercritical Environments," *Combustion Science and Technology*, Vol. 178, Nos. 1–3, 2006, pp. 49–100. doi:10.1080/00102200500292464

[10] Mayer, W., and Tamura, H., "Propellant Injection in a Liquid Oxygen/Gaseous Hydrogen Rocket Engine," *Journal of Propulsion and Power*, Vol. 12, No. 6, 1996, pp. 1137–1147. doi:10.2514/3.24154

[11] Yang, V., "Modeling of Supercritical Vaporization, Mixing and Combustion Processes in Liquid-Fueled Propulsion Systems," *Proceedings of the Combustion Institute*, Vol. 28, 2000, pp. 925–942. doi:10.1016/S0082-0784(00)80299-4

[12] Zong, N., Meng, H., Hsieh, S. H., and Yang, V., "Cryogenic Fluid Injection and Mixing Under Supercritical Conditions," *Physics of Fluids*, Vol. 16, No. 12, 2004, pp. 4248–4261.

doi:10.1063/1.1795011
[13] Bellan, J., "Supercritical (and Subcritical) Fluid Behavior and Modeling, Drops, Streams, Shear and Mixing Layers and Sprays," *Progress in Energy and Combustion Science*, Vol. 26, Nos. 4–6, 2000, pp. 329–366.
doi:10.1016/S0360-1285(00)00008-3
[14] Abramovich, G. N., *The Theory of Turbulent Jets*, MIT Press Cambridge, MA, 1963.
[15] Zong, N., and Yang, V., "Cryogenic Fluids, Jets and Mixing Layers in Transcritical and Supercritical Environments," *Combustion Science and Technology*, Vol. 178, Nos. 1–3, 2006, pp. 193–227.
doi:10.1080/00102200500287613
[16] Polikhov, S. A., and Segal, C., "Experimental Study of Subcritical to Supercritical Jet Mixing," 45th AIAA Aerospace Sciences Meeting and Exhibit, AIAA Paper 2007-569, Reno, NV, 8–11 Jan. 2007.
[17] Segal, C., and Polikhov, S. A., "Subcritical to Supercritical Mixing," *Physics of Fluids*, Vol. 20, No. 5, 2008, pp. 052101–052107.
doi:10.1063/1.2912055
[18] Chehroudi, B., and Davis, D. W., "Shear-Coaxial Jets from a Rocket-Like Injector in a Transverse Acoustic Field at High Pressures", 44th AIAA Aerospace Sciences Meeting and Exhibit, AIAA Paper 2006-758, Reno, NV, 9–12 Jan. 2006.
[19] Levya, I. A., Chehroudi, B., and Talley, D. G., "Dark Core Analysis of Coaxial Injectors at Sub, Near and Supercritical Pressures in a Transverse Acoustic Field," 45th AIAA Aerospace Sciences Meeting and Exhibit, AIAA Paper 2007-5456, Reno, NV, 8–11 Jan. 2007.
[20] Chehroudi, B., Talley, D. G., and Coy, E., "Initial Growth Rate and Visual Characteristics of a Round Jet into a Sub- to Supercritical Environment of Relevance to Rocket, Gas Turbine and Diesel Engines," 37th Aerospace Sciences Meeting and Exhibit, AIAA Paper 1999-0206, Reno, NV, 11–14 Jan. 1999.
[21] Polikhov, S. A., and Segal, C., "Two Phase Flow Supercritical Mixing," 44th Aerospace Sciences Meeting and Exhibit, AIAA Paper 2006-07566, Reno, NV, 9–12 Jan. 2006.
[22] Roy, A., and Segal, C., "Experimental Study of Subcritical to Supercritical Jet Mixing," 47th Aerospace Sciences Meeting and Exhibit, AIAA Paper 2009-809, Orlando, FL, 5–8 Jan. 2009.
[23] Yang., V., and Anderson, W., *Liquid Rocket Engine Combustion Instability*, Progress in Astronautics and Aeronautics Series, AIAA, Washington, DC, Vol. 169, 1995.
[24] Mayer, W., Telaar, J., Branam, R., and Schneider, G., "Characterization of Cryogenic Injection at Supercritical Pressure," 37th Joint Propulsion Conference and Exhibit, Salt Lake City, UT, 9–11 July 2001.
[25] Rodriguez, J. I., Levya, I. A., Chehroudi, B., and Talley, D. G., "Results on Subcritical One Phase Coaxial Jet Spread Angles and Subcritical to Supercritical Acoustically-Forced Coaxial Jet dark Core Lengths," 44th Joint Propulsion Conference and Exhibit, AIAA Paper 2008-4561, Hartford, CT, 21–23 July 2008.
[26] Levya, I. A., Chehroudi, B., and Talley, D. G., "Dark Core Analysis of Coaxial Injectors at Sub, Near and Supercritical Conditions in a Transverse Acoustic Field," 54th JANNAF Meeting, A566374, Denver, CO, 14–18 May 2007.
[27] Mayer, W., Schik, A., Vielle, B., Chauveau, C., Gokalp, I., Talley, D. G., and Woodward, R. G., "Atomization and Breakup of Cryogenic Propellants Under High Pressure Sub-Critical and Supercritical Conditions," *Journal of Propulsion and Power*, Vol. 14, No. 5, 1998, pp. 835–842.
doi:10.2514/2.5348

V. Yang
*Past Editor-in-Chief*